Reaction **Chemistry & Engineering**



View Article Online PAPER



Cite this: React. Chem. Eng., 2019, 4, 1779

Received 8th April 2019, Accepted 14th May 2019

DOI: 10.1039/c9re00152b

rsc.li/reaction-engineering

Jet-mixing reactor for the production of monodisperse silver nanoparticles using a reduced amount of capping agent†

Pinaki Ranadive, Aamena Parulkar and Nicholas A. Brunelli (1)*

Commonly used batch reactors for nanomaterial synthesis can be difficult to scale since rapid particle nucleation and growth require efficient mixing to produce monodisperse particle size distributions (PSD). Monodisperse particles can be synthesized through efficiently mixing the reactants in the liquid phase using a jet-mixing reactor. Using common synthesis precursors and concentrations, the jet-mixing reactor produces silver nanoparticles with a diameter of 5 ± 2 nm, as characterized by TEM, and a monomodal surface plasmon resonance (SPR) in the UV-vis spectrum. In comparison, a batch synthesis using the same concentrations of reactants produces nanoparticles with a diameter of 9 ± 4 nm and a bimodal SPR, indicating that jet-mixing produces a more monodisperse particle size distribution than batch synthesis. For the jetmixing synthesis, the concentration of the capping agent can be reduced to a value of 0.05 mM while retaining a narrow full-width of half-maximum (FWHM) of the SPR spectrum. Interestingly, decreasing the capping agent quantity from the standard concentration of 0.2 mM to 0.05 mM decreases the FWHM of the SPR, corresponding to a more monodisperse PSD at lower capping agent concentration. This result is attributed to the increased stabilization at lower ion concentrations in the solution. For low capping agent concentrations, additional experiments adding small amounts of sodium nitrate support this observation. Overall, the jet-mixing reactor represents a viable system for the continuous production of size-controlled silver nanoparticles with reduced amounts of capping agent.

1. Introduction

Important materials discoveries continue to emerge as the ability to generate nanomaterials with exquisite control on the lab scale advances. However, translating these exciting discoveries into commercial processes offers considerable challenge, especially because of the difficulties associated with scalability of small-scale synthetic techniques. Indeed, many of these nanomaterials are synthesized in small scale batch processes that allow precise control over many important synthetic conditions, including reaction temperature, mixture composition, and other parameters that can affect the final size distribution and even the morphology of the nanoparticles (NPs) formed.1 The mixing dynamics in the reaction system directly influence the ability to control these parameters. For small scale synthesis, it is possible to control these different parameters sufficiently to produce nanomaterials with a monodisperse particle size distribution

The Ohio State University, William G. Lowrie Department of Chemical and Biomolecular Engineering, 151 W. Woodruff Ave., Columbus, OH 43210, USA. E-mail: brunelli.2@osu.edu: Web: www.twitter.com/OSUChemEProfBru † Electronic supplementary information (ESI) available. See DOI: 10.1039/ c9re00152b

(PSD). However, scaling up these syntheses to produce larger quantities of nanomaterials often results in complications since controlling synthetic parameters for batch methods when operating at larger length scales is difficult.2 Thus, it remains a challenge to develop methods for the scalable manufacturing of nanoparticles with the same quality as achieved in small-scale synthesis.

The synthesis of nanomaterials is commonly accomplished using liquid-phase methods. Since liquid-phase methods are broadly applicable to many materials,3 advances in nanomaterial synthesis can be achieved through investigating a single material. A convenient system to investigate is the production of silver nanoparticles. Silver nanoparticles have many applications, including as biosensing and bioimaging agents,4,5 catalysts in several reactions, and antimicrobial additives.^{5,6} Silver nanoparticles are a convenient system to investigate since they exhibit a localized surface plasmon resonance (SPR), in which the interaction of light with the electrons in the conduction band of an Ag particle results in a specific resonant oscillation.7 The frequency of this oscillation provides information about several properties of the NP colloid, including particle size and shape.^{8,9} The frequency falls into the visible range of the electromagnetic spectrum for nanomaterial systems such as Ag and Au, and

hence can be characterized by UV-vis spectroscopy. Interestingly, the extent of broadness of the SPR spectrum, measured by its full width at half maximum (FWHM), is indicative of the polydispersity of the sample. Generally, a broader PSD will have a larger FWHM in the UV-vis spectrum.

Typically, these metal nanoparticles are synthesized by the injection of a reducing agent into a solution containing a nanoparticle precursor to induce nanoparticle nucleation and growth.³ Each of the components in the mixture needs to be balanced carefully since the concentration of each can impact the final product properties, including the particle size and the PSD. Controlling the PSD is important since the NP performance is often a function of size. Although not all applications require monodisperse PSDs, 11 most applications benefit from having monodisperse particle sizes. For example, a recent study demonstrated that large Ag nanoclusters were more selective for the partial oxidation of propylene. 12 In addition to the performance of NP, a uniform PSD can also affect the stability of NP solutions. A monodisperse PSD tends to increase the colloidal stability of the distribution postsynthesis according to derivations of the classical nucleation theory (CNT), limiting particle growth phenomena such as Ostwald ripening.3 This can be important as the colloidal stability can affect the shelf life for these materials.

Synthesizing NPs with a well-characterized and stable PSD can be challenging since the PSD can broaden either during or after the synthesis, making it necessary to prevent aggregation and Ostwald ripening from altering the PSD. Two common methods to control PSD are using reverse micelles and using capping agents. 13-16 Reverse micelles utilize surfactants to produce a bi-phasic system consisting predominantly of an organic phase with dispersed droplets of an aqueous phase containing the reactants. The organic medium between micelles isolates NPs, preventing agglomeration¹⁵ and allowing control over the final particle size.16 However, the requirement of an organic solvent makes reverse micelles biologically and environmentally less friendly. In contrast, nanoparticle synthesis can be accomplished in a single phase through utilizing capping agents. Capping agents are ionic species or bulky molecules that provide an electrostatic or steric barrier, respectively, between individual NPs in solution to prevent agglomeration. This method is a preferred choice in toxicity studies17 and is also used by commercial vendors. 12,13

The beneficial aspects of utilizing a capping agent need to be balanced with the cost of the capping agent when considering the scalable manufacture of nanomaterials. From an economic perspective, the amount of capping agent utilized should be the minimum that can produce the desired product quality. From a scientific perspective, the concentration of the capping agent plays an important role in determining NP stability. At too low of a capping agent concentration, the surface of the NPs is not sufficiently "capped" and aggregation takes place because of van der Waals attraction. Interestingly, it can be problematic to use an excessive amount of capping agent since many common capping agents like

trisodium citrate (TSC) are ionic. At high concentrations, the capping agent can dissociate in solution, increasing the ion concentration of the solution. According to the DLVO theory, high ion concentration can lower the electrostatic barrier between two particles, promoting aggregation. 18,19 Hence, it is hypothesized that there is a "just right", concentration of capping agent at which NPs may remain stable. At this intermediate concentration, steric or electrostatic repulsion prevents aggregation, leading to stable colloidal nanoparticles in solution. Besides affecting NP stability, capping agents remaining in solution can also have other undesired effects such as altering the particle morphology^{1,21} or hindering catalytic activity.²² Most importantly, considering the holistic goal of scaling up NP syntheses, reducing the amount of capping agent used can reduce the overall process cost. Hence, it is desirable to optimize the amount of capping agent used for synthesizing a monodisperse PSD. Current synthetic methods report utilization of capping agent concentrations that are equal to or higher than the concentration of metal precursor in solution. 10,13,16-22,24,27,30 It is unclear if this concentration represents an optimum for the synthesis or is the concentration required for batch processes to maintain a narrow PSD.

In addition to using an optimal amount of capping agent, a narrow PSD requires creating uniform reaction conditions to enable uniform nucleation and growth. Uniform conditions can be generated through inducing intense mixing to reduce the timescale for mixing (τ_{mix}) below the timescale for reaction (τ_{reaction}). For solution-phase Ag NP synthesis, the process involves the reduction of Ag⁺ ions to Ag⁰ atoms that nucleate and grow to form NPs. The reduction is commonly achieved through using a reducing agent³³ such as NaBH₄ (ref. 34-37) that is highly active and reacts on the timescale of milliseconds.³⁸ This rapid reaction time makes it necessary to create intense mixing so that uniform reaction conditions can be obtained. When scaling up the batch process, it is challenging to generate the intense mixing necessary to produce a narrow PSD, often resulting in batch-to-batch variability. 39,40

Efficient mixing requires controlling the process at all spatial scales, including macromixing, mesomixing, and micromixing.41 Macromixing refers to achieving composition homogeneity within the bulk of the fluid, mesomixing occurs at the different scales of eddies in the fluid, and micromixing at the molecular level between fluid lamellae. Each spatial scale has an associated time-scale that add in series to comprise the overall τ_{mix} . In a batch reactor, the volume is large enough that the overall mixing process can be limited by macromixing.² Poor macromixing in batch reactors can cause non-uniformity in the reactant concentrations and temperature throughout the volume of the batch. Hence, fast reactions such as redox or neutralization reactions, progress with different rates spatially in the reactor, 42 resulting in a wide PSD for NP synthesis solutions. From previous work for colloidal syntheses, a direct link exists between $\tau_{\rm mix}$ and the PSD of the NPs synthesized. 43 The importance of macromixing can be mitigated through reducing the dimensions of the reactor as is possible in microfluidic and millifluidic devices. ⁴⁴ Microfluidic technologies for nanoparticle synthesis take advantage of the small $\tau_{\rm mix}$ that is a result of their compact volume. ^{45,46} While continuous flow microfluidic devices can obviate macromixing, it is still important to achieve efficient mesomixing and micromixing when using highly active reducing agents.

Several continuous syntheses at both ambient conditions and high temperatures, and in gas and liquid phase, have been explored for Ag NPs. 28,32,47-55 Two notable geometries are a coaxial mixing system and an impinging jet reactor. The coaxial mixing system used high flow rates to increase mixing and produce nanoparticles⁴⁸ that would be promising if issues with radial mixing can be overcome. The impinging jet reactor was able to prevent clogging, but the size distribution obtained by the continuous process was broad. 49 Continuous flow synthesis of nanomaterials would be promising if the reactor could achieve better mixing dynamics. Another reactor type, the segmented flow reactor is known to offer a narrow size distribution because of minimized axial dispersion, but liquid cross-mixing between individual segments because of menisci on the walls may actually broaden the PSD. 52,56 Recently, our research group demonstrated the continuous synthesis of zeolitic imidazolate frameworks (ZIFs) using a continuous jet-mixing reactor.⁵⁷ The jet-mixing reactor enabled efficient mixing for the rapid nucleation and growth of ZIFs, resulting in narrow PSD that caused the ZIFs to be stable colloidal suspensions. The jet-mixing reactor also had a small reactor volume that efficiently synthesized the nanomaterials with high yields and high productivities.

In this work, the jet-mixing reactor is used to synthesize Ag NPs in a continuous manner. The nanoparticles are analyzed using common characterization methods, including transmission electron microscopy (TEM), Ultraviolet-visible absorption (UV-vis) spectroscopy, and dynamic light scattering (DLS). The properties of Ag NPs obtained by batch synthesis are compared to those obtained by jet-mixing synthesis. Both the batch and jet-mixing synthesis are examined for batch-to-batch variability. For the jet-mixing reactor, the effect of the flow rate, the concentration of the reducing agent, and the capping agent on the PSD of Ag NPs is examined. With the jet-mixing reactor, a reduced capping agent concentration is found to be sufficient to stabilize the nanoparticles. To understand the stabilization, experiments are conducted to study the effect of the ion concentration of the solution. Overall, this work demonstrates that the jet-mixing reactor is a promising continuous system for the synthesis of silver nanoparticles.

2. Experimental methods

2.1. Chemicals

All chemicals are used as received without further purification, including: silver nitrate (AgNO₃; >99%, ACS grade; VWR Life Science), trisodium citrate dihydrate (TSC; > 99%, ACS

grade, BDH Chemicals), sodium nitrate (NaNO₃; 98% Beantown Chemical), and sodium borohydride (NaBH₄) solution (12 wt%) in 14 M NaOH (Sigma Aldrich). All solutions are prepared using deionized (DI) water.

2.2. Reactor design

The design of the reactor has been adapted from a gas-phase synthesis⁵⁸ and has been used by our group for successful ZIF-8 synthesis in liquid phase.⁵⁷ The reactor design and assembly are shown in Fig. 1. The reactor is manufactured inhouse from a thermally and chemically resistant polyether ether ketone (PEEK) cube $(1" \times 1" \times 1")$. The cube consists of three cylindrical flow channels (one main line and two jets) that intersect in a perpendicular manner in the center of the device. A flow channel with diameter (d_{main}) of 0.04 inch (1.02 mm) goes through the entire length of the reactor and is called the main line. Two identical jet lines with a diameter (d_{iet}) of 0.02 inch (0.51 mm) impinge perpendicularly at the center of device with the main line. Although the jets impinge from opposite sides of the main line, both jet lines are drilled starting from one side of the cube to ensure that the jet lines are properly aligned, as has been done for confined impinging jet reactors.41 The channels are threaded at the ends to enable connection of clear polytetrafluoroethylene (PTFE, ID 0.03") tubing using appropriate microfluidic PEEK fittings. The main line delivers the reducing agent solution while the jet-line delivers the silver substrate and capping agent solution. The reactants are pumped using two KD Scientific 100KD syringe pumps. For the jet lines, a Y-adapter is used to split the flow from the syringe pump into two streams, each of which connects to one of the jets. From control experiments, it has been determined that Ag NP synthesis is insensitive to differences in flow between the two jets (section 5). The combined jet lines and main line flows comprise the product solution that flows out downstream of the reactor. The outlet product stream is collected in a flask covered with aluminum foil and stored in an ice bath.

2.3. Batch synthesis of silver nanoparticles (Ag NPs)

Initial studies involve comparing Ag NPs synthesized using concentrations utilized for batch methods reported

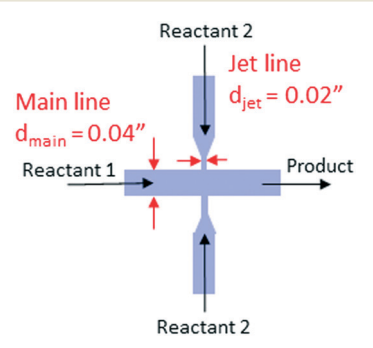


Fig. 1 The reactor design showing the main line ($d_{\rm main} = 0.04$ ") carrying reactant 1 and orthogonal jet lines ($d_{\rm jet} = 0.02$ ") carrying reactant 2. The product is collected downstream of the reactor.

previously. 36,59 For the Ag NP synthesis, an aqueous solution of 0.2 mM AgNO₃ and 0.2 mM TSC is prepared at room temperature. An equal volume of aqueous solution of 0.6 mM NaBH₄ is prepared. The NaBH₄ solution is prepared in an ice bath and cooled for 20 minutes before use. All batch experiments are carried out in a 250 mL round-bottom flask. In a standard batch synthesis, 50 mL of the NaBH₄ (0.6 mM) solution that has been cooled is placed in the 250 mL flask and stirred at 200 RPM using a PTFE-coated stir bar. To this solution is added the AgNO3 and TSC solution (50 mL). As previous literature reports, stirring is stopped after 2 minutes and the solution is stored in the refrigerator at 4-6 °C. 16,60 Further details on the synthesis procedure can be found in the ESI† (section 1). A different order of reagent addition, involving the addition of the NaBH4 solution to the AgNO3 and TSC solution in batch, is also tested. Both methods produce comparable nanoparticles, as suggested by the UV-vis spectra in Fig. S14.†

2.4. Flow synthesis of silver nanoparticles using a jet-mixing reactor

The standard jet-mixing synthesis is performed using a solution with concentrations of 0.2 mM AgNO3 and 0.2 mM TSC in water and a separate solution with 0.6 mM NaBH4 in water. The solutions are loaded into separate syringes. The syringe with NaBH4 is connected to the main line and the silver salt and TSC solution is connected to the jet line. For the standard experiment, the syringe pumps are set to a flow rate of 48 mL h⁻¹. These are the flow rates that are determined to provide sufficiently intense mixing to produce a monodisperse PSD, as shown in the ESI† in Fig. S1. The experiment to find these flowrates is described in the ESI† (section 2). The beaker in which the jet-mixing product is collected is placed in an ice bath. The collection beaker in jet-mixing or the round-bottom flask in batch are both covered with aluminum foil to limit photolytic reduction of AgNO₃.60 Further details on the synthesis procedure can be found in the ESI† (section 1.1 and 1.3).

2.5. Material characterization

All analyses are performed within one hour of synthesis. The product Ag NP solution is characterized primarily via UV-vis, DLS, and TEM. UV-vis analysis is performed using a ThermoFisher Evolution 300 UV-vis spectrophotometer with a xenon lamp using a bandwidth of 2 nm and a scan speed of 600 nm min⁻¹. After the particles have been synthesized, the product solution (1 mL) is diluted with DI water (1 mL) in a 1 cm pathlength quartz cuvette. Fifteen minutes after synthesis, the UV-vis spectrum for the sample is recorded. The data are analyzed through fitting the data to determine the wavelength maximum (λ_{max}) and the full width at half maximum (FWHM) of the UV-vis spectrum, as described in the ESI† (section 3). The PSD is also investigated using DLS analysis using a Brookhaven Instruments Corporation BI-200SM Goniometer. The sample (1 mL) is filtered using a 0.2 µm PTFE syringe filter before DLS is performed using a 637 nm laser beam at a detector angle of 90° with a dust cut-off of 20 µm. The solvent is set as water and the temperature as 20 °C. Three runs are conducted for each sample with the average being recorded to calculate the PSD. Analysis is done via the Brookhaven Instruments Dynamic Light Scattering software. For most samples, the PSD is corroborated through using a FEI Tecnai G2 Spirit TEM at a voltage of 80 kV and magnification of 115 000× in bright-field mode. TEM samples are prepared on 150 mesh holey-carbon copper grids by dropping 15 μL of sample on the grid 1 hour after collection and letting dry for up to 2 hours in a partially covered Petri dish to prevent contamination. Particle size analysis is performed using ImageJ software. 61 More information about the analysis is included in the ESI† (section 3).

3. Results and discussion

3.1. Theoretical comparison of the mixing time scales in the batch and jet-mixing reactor

The mixing time (τ_{mix}) can be estimated for an idealized turbulent mixer as:

$$\tau_{\text{mix}} = 3.3 \left(\frac{ML^2}{P}\right)^{\frac{1}{3}} \tag{1}$$

where, M is the mass of fluid in the dissipation region, L is the characteristic length of the dissipation region, and P is the mechanical power introduced into the dissipation volume. The power input into the system is the total kinetic energy of the incoming main line (diameter, $d_{\text{main}} = 0.04''$) stream with flowrate Q_0 and velocity v_0 , and the incoming jet line (diameter, $d_{jet} = 0.02''$) stream with total flowrate Q_1 and velocity v_1 . Hence, P can be expressed as:

$$P = \sum \rho v_i^2 Q_i \tag{2}$$

L can be estimated as the diameter of the jet line Combining these into (1), τ_{mix} can be expressed as:

$$\tau_{\text{mix}} = 3.3 \left(\frac{\frac{1}{32} \pi^2 d_{\text{main}}^2 d_{\text{jet}}^3}{\frac{Q_0^3}{d_{\text{main}}^4} + \frac{4Q_1^3}{d_{\text{jet}}^4}} \right)^{\frac{1}{3}}$$
 (3)

For the standard flowrates $(Q_0 = Q_1 = 48 \text{ mL h}^{-1})$ used for synthesis, the estimated τ_{mix} is 22 ms.

In comparison, it has been estimated that for a 250 mL cylindrical flask (diameter = 55 mm), the time for 95% mixing of a water-like fluid with a 2.5 cm magnetic stir-bar at 500 RPM, is $\tau_{\text{mix}} = (8.3 \pm 1.4)$ s. This suggests that for Ag NP synthesis, the τ_{mix} for the batch reactor is over two orders-ofmagnitude slower than for the jet-mixing reactor operating at standard conditions.

Experimentally, it is found that increasing the mixing time in the jet-mixing reactor by operating at a main line and jet line flowrate of 2 mL h⁻¹ with standard reagent concentrations results in an Ag NP sample that has a UV-Vis spectrum with its FWHM approaching that of a standard Ag NP batch, suggesting that the mixing time plays an important role in Ag NP monodispersity. The data are included in Fig. S1.†

3.2. Standard batch and jet-mixing synthesis

Initial work with the jet-mixing reactor demonstrates the successful synthesis of Ag NPs using the standard concentrations of 0.2 mM AgNO₃, 0.2 mM TSC, and 0.6 mM NaBH₄. The silver nanoparticles produced in the jet-mixing reactor are characterized by UV-vis, TEM imaging, and DLS. As can be observed in Fig. 2, the UV-vis spectrum has a single sharp peak that is consistent with a narrow PSD. The spectrum can be fit to obtain both the absorbance maximum (λ_{max}) and the full-width at half-maximum (FWHM). For the standard conditions with the jet-mixing reactor, the particles are found to have a λ_{max} = 389 nm and a FWHM = 57 nm, which is consistent with a monodisperse PSD.

The actual PSD for this synthesis is investigated using TEM to corroborate the UV-vis spectrum. Several images (Fig. 3a shows a representative TEM image; additional images are shown in Fig. S5 \dagger) are taken from different locations on the TEM grid, with over 300 particles being used for PSD analysis. Using ImageJ software, ⁶¹ it is determined that the jet-mixing reactor produces a monodisperse distribution with a mean particle size of 5 \pm 2 nm. The particle size measured with TEM is consistent with the UV-vis spectrum. While TEM imaging is useful to directly visualize particles, TEM sample

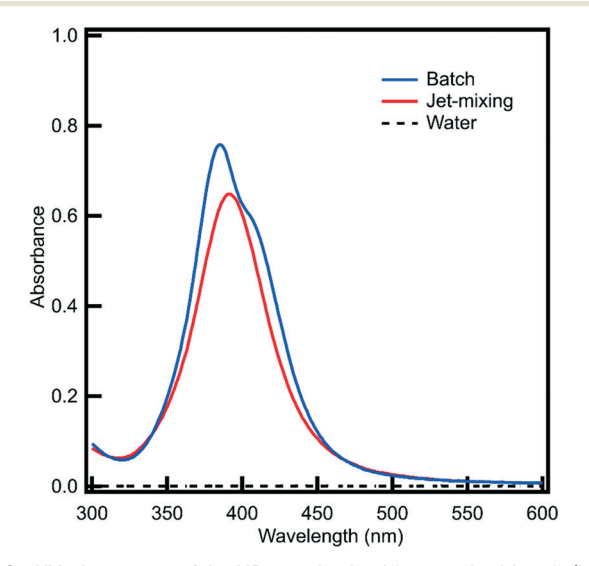


Fig. 2 UV-vis spectra of Ag NPs synthesized by standard batch (blue) and jet-mixing (red) synthesis. Synthesis conditions are as follows: $Q_r = Q_j = 48 \text{ mL h}^{-1}$ for jet-mixing; [NaBH₄] = 0.6 mM, [AgNO₃] = 0.2 mM, [TSC] = 0.2 mM for both syntheses.

preparation and analysis are resource intensive, making it desirable to characterize the PSD with alternative methods such as DLS. Analyzing the jet-mixing synthesis with DLS reveals a PSD of 7 ± 2 nm. As DLS measures the hydrodynamic diameter of the particle, it is expected to be greater than the size obtained by TEM. While the size measured via DLS is only slightly greater than that obtained via TEM, the close match suggests that the combination of UV-vis and DLS can be used to characterize the silver nanoparticles with TEM providing corroborating evidence. The DLS data are shown in Fig. S6 and Table S2.†

For comparison, the standard synthesis concentrations are used in a batch process and result in the formation of nanoparticles. These are characterized using UV-vis (Fig. 2), TEM (Fig. 3b), and DLS (Fig. S6 and Table S2†). The UV-vis spectrum is shown in Fig. 2. Similar to the jet-mixing sample, the UV-vis spectrum has a prominent surface plasmon resonance (SPR) peak, confirming the synthesis of Ag NPs. While the UV-vis spectrum has a sharp peak at a λ_{max} = 389 nm, it also has a shoulder at 410 nm. Since it is generally established that a longer wavelength of absorption corresponds to a larger particle size²⁹ or a non-spherical morphology,²³ the shoulder in the UV-vis spectrum suggests the coalescence of particles. Comparing the nanoparticles made with batch and jet-mixing methods, the two spectra have similar intensities, but the batch synthesis results in a bimodal distribution with a broader UV-vis spectrum. These batch samples are also investigated with TEM to determine the PSD, as shown in Fig. 3b. From multiple TEM images, the PSD calculated from analyzing over 300 particles is found to be 9 ± 4 nm. Consistent with the UV-vis data, this PSD appears to have a primary particle population around 8 nm and an extended tail of larger particles between 16 and 20 nm. In addition to Fig. 3b, other TEM images used for PSD calculation using ImageJ are shown in Fig. S7.† The PSD from DLS is 13 ± 3 nm, which is comparable with the PSD determined from TEM images. The DLS data are shown in Fig. S6 and Table S2.†

In comparison to batch synthesis, the jet-mixing reactor produces a more uniform PSD, as is evidenced by comparing the size distribution obtained from TEM. This observation indicates the τ_{mix} is an important consideration for Ag NPs. It is thought that a secondary stage of particle formation is avoided by using jet-mixing in comparison to batch, as indicated by the UV-vis spectra of the samples produced using the two methods. Further, it is observed that the jet-mixing synthesis produces a smaller mean particle size than the batch process. This is attributed to the efficient micromixing in the jet-mixing reactor that creates uniform nucleation conditions that induces a higher rate of nucleation. Since the total available silver substrate is limited, the formation of a greater number of nuclei results in the growth of the nuclei being limited. This observation of a smaller particle size being produced via microreactor synthesis as compared to batch, has been reported for other microfluidic Ag NP syntheses.37,62 The obtained sizes for the batch and jet-mixing

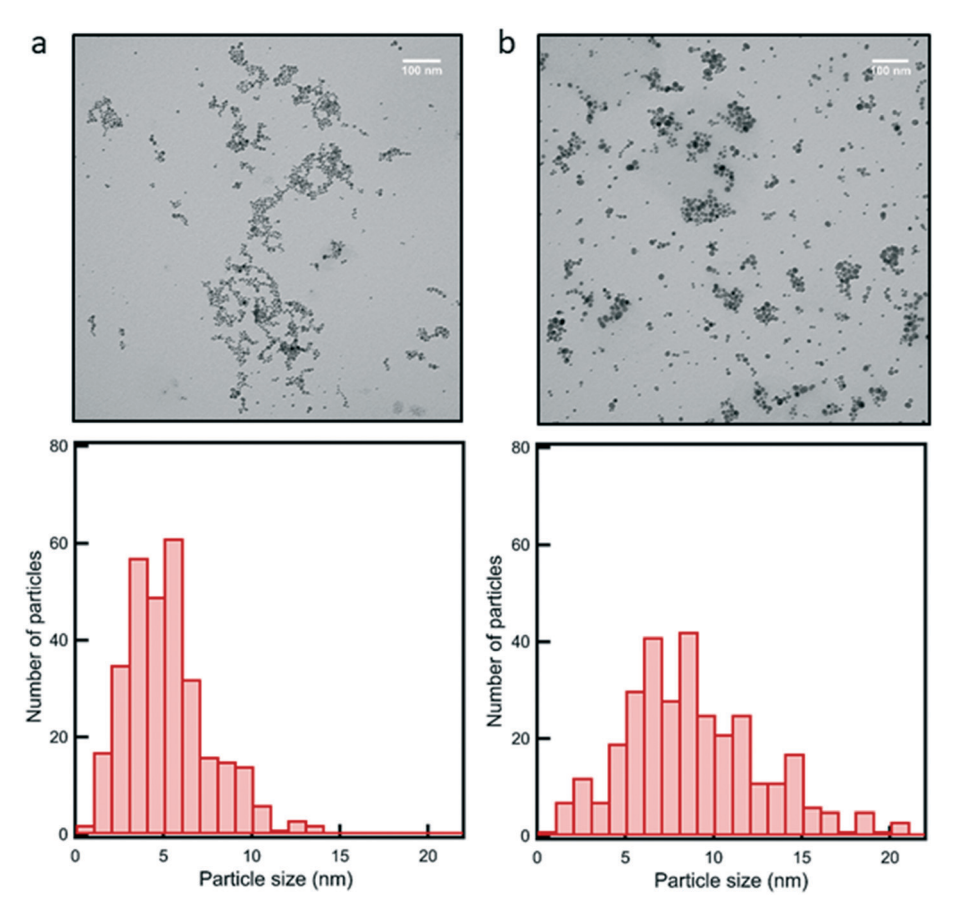


Fig. 3 TEM images and corresponding PSDs of standard (a) jet-mixing (5 ± 2 nm) and (b) batch (9 ± 4 nm) syntheses. The distributions are calculated by the size analysis of 300 particles for each synthesis, using ImageJ software. Synthesis conditions are as follows: $Q_r = Q_i = 48$ mL h⁻¹ for jet-mixing; [NaBH₄] = 0.6 mM, [AgNO₃] = 0.2 mM, [TSC] = 0.2 mM for both syntheses.

synthesis are in agreement with those previously reported in literature. 37,48,49,62-64 NaBH4 being among the more active reducing agents typically results in faster reaction kinetics, leading to rapid nucleation and a small particle size (<10 nm). Among the microfluidic syntheses with a mean size of 3-5 nm, the standard deviation obtained varies between 30-50%. The PSD obtained from the jet-mixing reactor for standard operating conditions falls within this range.

Along with monodispersity, another important consideration for the synthesized Ag NPs is particle yield. The absorbance associated with the SPR peak of the Ag NPs, obtained from the UV-vis spectrum, can be correlated with NP concentration using Beer's law.29 Using this method, the yield for the batch and jet-mixing synthesis is calculated to be 88% and 82% respectively, suggesting that the material efficiency of the two processes is comparable. The detailed calculation of yield is outlined in the ESI† in section 4.

3.3. Reproducibility tests for the jet-mixing synthesis

One of the main advantages of a flow synthesis over a batch synthesis is the potential to achieve greater reproducibility in the synthesis conditions (i.e., mixing) to eliminate batch-tobatch variability. Specifically, it is desirable to demonstrate that the reactor performs (1) stably over a single continuous test and (2) consistently across different tests. For Ag NPs, UV-vis is a facile method to test variability between properties across different samples by comparing the λ_{max} and FWHM of the SPR absorbance peak.

Initially, the continuous steady-state operation of the jetmixing reactor is tested by checking the variability within a single continuous run. The UV-vis spectra from a standard jet-mixing Ag NP synthesis over its run-time (i.e., start of the synthesis to end of the synthesis) are monitored to ensure that the Ag NPs synthesized in a continuous run have similar properties at different sampling times. The product solution from an hour-long run is collected intermittently every 15 minutes and analyzed by UV-vis after collection. The absorbance, λ_{max} and FWHM are noted for each sample. The UVvis spectra overlap for each sample collected (samples S1 to S5) shown in Fig. 4, indicating that Ag NPs with similar properties are formed at all times. Quantitatively, the standard deviation of the properties of the UV-vis spectra between the various samples is <5%, corroborating the uniformity in Ag NP properties. The data are reported in Table S3.†

Next, multiple batch and jet-mixing runs with the standard reagent concentrations are conducted to compare the variability across the runs for the two synthesis methods

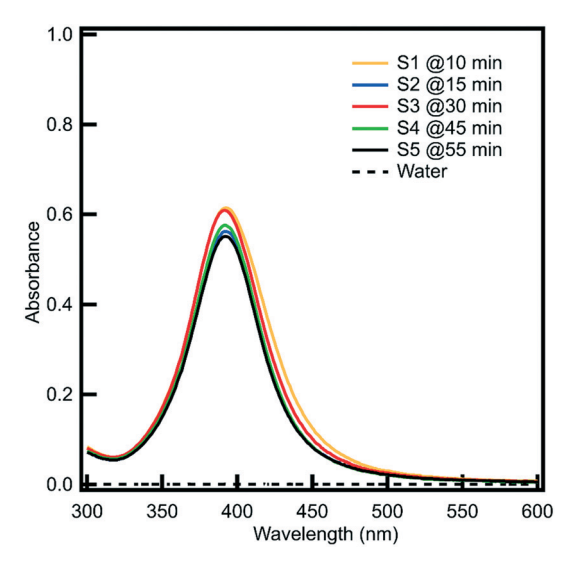


Fig. 4 UV-vis spectra of Ag NP samples collected at various times during a standard jet-mixing run. The legend Sn @t min indicates the nth sample collected at time t min after starting run. Synthesis conditions are as follows: $Q_r = Q_i = 48 \text{ mL h}^{-1}$; $[NaBH_4] = 0.6 \text{ mM}$, $[AgNO_3]$ = 0.2 mM, [TSC] = 0.2 mM.

using the standard conditions for each method. Each synthesis is analyzed by UV-vis. It is observed that for batch synthesis, the UV-vis spectra vary from batch to batch despite efforts to maintain all synthesis parameters constant. This is qualitatively indicated by Fig. 5a for six different runs attempted using identical conditions. Quantitatively, the variability between batches is greater than 5% for the FWHM and the intensity of the UV-vis spectrum, as indicated by the standard deviation of the parameters for all runs. The quantitative variability in these parameters is provided in Table S4.† A similar experiment with the jet-mixing reactor shows lesser variability between six identical runs, as is qualitatively shown in Fig. 5b, demonstrating its ability to produce Ag NPs with consistent properties over multiple separate runs. The quantitative variability in these parameters is provided in Table S5.† It is hence concluded that jet-mixing results in more reproducible synthesis of Ag NPs with monodisperse narrow PSD as compared to batch synthesis.

3.4. Effect of synthesis parameters in jet-mixing synthesis

The synthesis of nanoparticles can be tuned by modifying several reaction parameters for jet-mixing synthesis, the sodium borohydride concentration ([NaBH₄]) and the capping agent concentration ([TSC]). From a commercial perspective, it is desirable to minimize the amounts of the different components to reduce cost while still maintaining product quality. The reducing agent influences the reaction rate. Excess reducing agents increase synthesis cost and may also contribute to higher ion concentration in solution, causing eventual agglomeration of NPs.65 To determine if an optimum concentration for NaBH4 exists to achieve monodisperse Ag NPs while limiting the reagent concentration used, the standard jet-mixing synthesis is performed by varying the NaBH4 concentrations between 0.03 mM, the stoichiometric amount⁴⁸ to 2.4 mM. The concentrations of AgNO3 and TSC are maintained at 0.2 mM each. It is observed that the FWHM narrows when using increasing concentrations of NaBH₄. The most significant decrease in FWHM occurs for low NaBH₄ concentrations whereas the FWHM changes less above a NaBH₄ concentration of 0.6 mM. This suggests that the standard concentration of NaBH4 used for this work (0.6 mM) is effective. A summary of the FWHMs calculated from the UVvis spectra of all runs for varying NaBH4 concentration are reported in Table S6.†

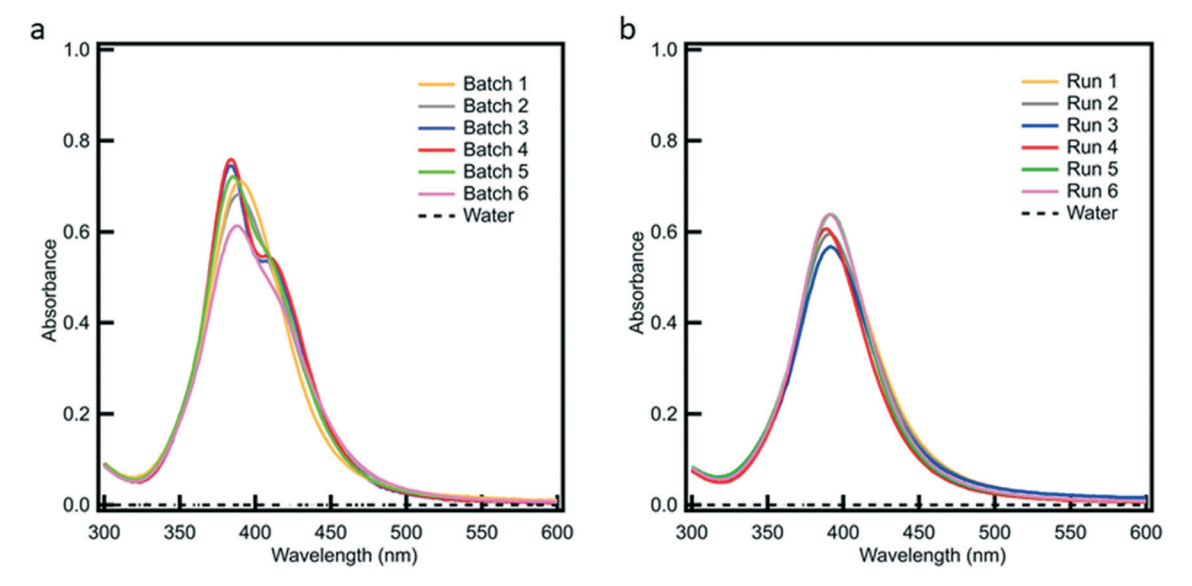


Fig. 5 UV-vis spectra of six separate runs of Ag NP synthesis in a standard (a) batch synthesis in a 250 mL round bottom flask at 200 RPM; (b) jetmixing synthesis with NaBH₄ solution flowing through the main line at 48 mL h⁻¹ and AgNO₃ + TSC solution flowing through the jet line at 48 mL h^{-1} . Synthesis conditions are as follows: [NaBH₄] = 0.6 mM, [AgNO₃] = 0.2 mM, [TSC] = 0.2 mM for both syntheses.

The second parameter investigated is the effect of capping agent concentration on NP synthesis. The capping agent represents an important component to help stabilize nanoparticles in solution and prevent agglomeration. An optimum capping agent concentration has also been previously reported for Ag NP batch synthesis. 19 In a synthesis in which TSC acts solely as the capping agent, it is shown that varying the concentration of TSC from 0.05 mM to 1.5 mM results in agglomeration at low concentrations, coalescence at high concentrations, and an intermediate concentration of the order of 0.1 mM results in NPs with a narrow PSD. However, other works show a linear trend where the PSD is seen to increase or stay constant with an increase in the TSC concentration.62

For the jet-mixing reactor, the effect is studied of TSC concentration on PSD of Ag NPs. The standard jet-mixing Ag NP synthesis is performed using different concentrations of TSC, ranging from 1 µM to 0.8 mM. Each sample is analyzed by UV-vis, and the FWHM of the spectrum is calculated, as shown in Fig. 6. It is observed that the FWHM decreases as the concentration of TSC is increased from 0.001 mM to 0.05 mM and increases again as the TSC concentration is increased further. The summary of FWHMs obtained for multiple jet-mixing runs conducted for different capping agent concentrations has been listed in Table S7.† Comparing this different reported result to many Ag syntheses, 10,13,16,23,25-28,31,32 the jet-mixing reactor is able to produce uniform Ag NPs with a low molar ratio of capping agent to silver substrate, as shown in Fig. 7. The concentration of capping agent that results in the narrowest FWHM is 0.05 mM. This is less than the typical concentration used for batch synthesis by a factor of four.

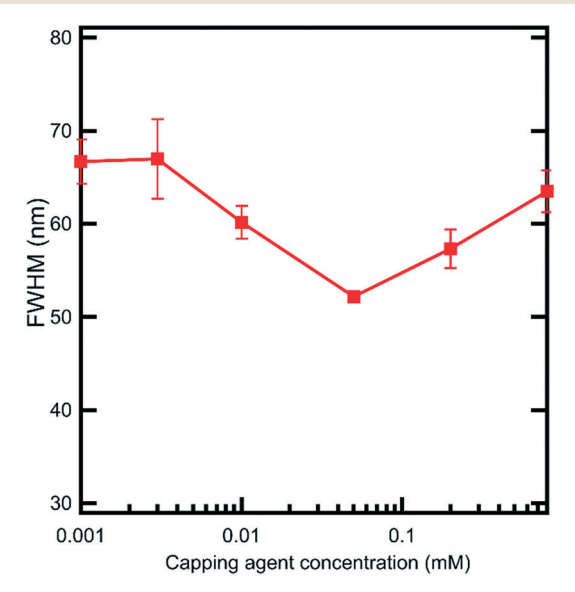


Fig. 6 Comparison of FWHM of Ag NPs synthesized via jet-mixing, calculated from UV-vis spectra, against the TSC concentration (mM) used in the run. The TSC concentration is varied while keeping other synthesis conditions at the following values: $Q_r = Q_j = 48 \text{ mL h}^{-1}$; $[NaBH_4] = 0.6 \text{ mM}, [AgNO_3] = 0.2 \text{ mM}.$

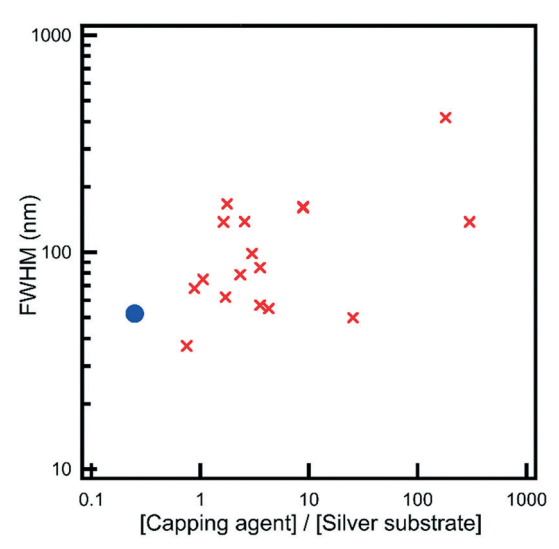


Fig. 7 Plot summarizing the FWHM of Ag NPs, obtained for different molar ratios of capping agent to silver substrate. The data includes a number of studies from literature (red) and the data obtained in this work (blue). Jet-mixing synthesis results in a narrow FWHM of 55 nm while requiring a low capping agent concentration of 0.05 mM. Other synthesis conditions are as follows: $Q_r = Q_i = 48 \text{ mL h}^{-1}$; [NaBH₄] = 0.6 mM, [AgNO₃] = 0.2 mM. The capping agent to silver substrate molar ratios have been calculated based on parameters such as % vol., weight, or molar concentration of the Aq NP precursors reported in previous works. 10,13,16,23,25-28,31,32

It is interesting to investigate how the batch synthesis performs at the optimum concentration obtained for jet-mixing. A batch synthesis comparable to the jet-mixing synthesis at 0.05 mM TSC is carried out and analyzed by UV-vis. The spectrum obtained for batch is compared against that for jetmixing in Fig. 8. For the batch synthesis using 0.05 mM

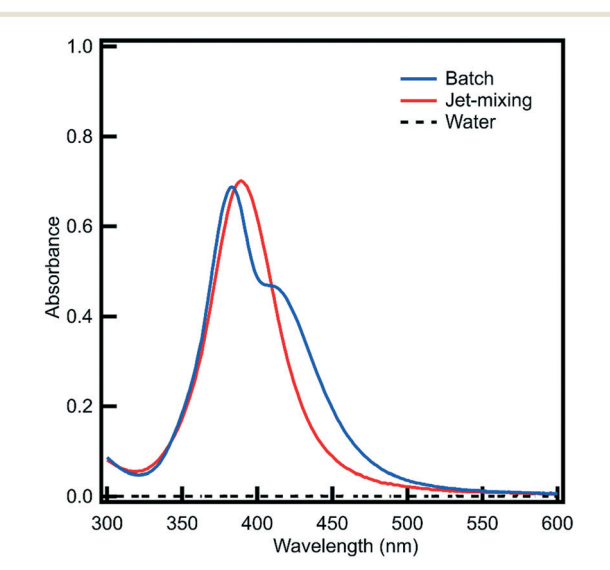


Fig. 8 UV-vis spectra comparing batch (blue) and jet-mixing (red) syntheses at 0.05 mM TSC; the optimum concentration obtained for jetmixing. Other synthesis conditions are as follows: $Q_r = Q_i = 48 \text{ mL h}^{-1}$ for jet-mixing; $[NaBH_4] = 0.6$ mM, $[AgNO_3] = 0.2$ mM for both syntheses.

capping agent, the synthesis mixture has a UV-vis spectrum that is bi-modal, suggesting that insufficient TSC is present to prevent agglomeration. However, the jet-mixing synthesis remains monomodal at 0.05 mM TSC. This observation is supported by representative TEM images of batch and jet-mixing syntheses at 0.05 mM TSC, shown in Fig. S9.† From analyzing over 100 particles for each sample, the PSD is found to be 8 \pm 5 nm for batch and 7 \pm 2 nm for jet-mixing. This indicates that mixing plays an important role in governing the effectiveness of the capping agent.

An interesting observation to note in Fig. 6 is the increase in the polydispersity of the Ag NPs synthesized at TSC concentrations above 0.05 mM, as indicated by the FWHM. It is hypothesized that this is associated with an increase in the ion concentration of the solution. TSC is an anionic surfactant with three carboxyl groups each bonded to a sodium ion. On dissolving in a polar solvent such as water, the carboxylate salt in excess of that required for capping would dissociate into the sodium ions and the carboxyl capping moiety. Any increase in the TSC concentration above 0.05 mM should hence lead to a three-fold increase in the ion concentration in the solution, which has been known to cause agglomeration for other systems. 18,65 The effect of the ion concentration in the solution on PSD is investigated through a series of experiments adding sodium nitrate (NaNO₃) to the reaction system. NaNO₃ is chosen as the salt as the ions Na⁺ and NO₃ are already present in solution and will not react with other ions in solution, as compared to ions such as Cl, which if added would cause precipitation of AgCl. Initially, the ion concentration is increased prior to synthesis. NaNO₃ of equal concentration (32 mM) is added to each of the standard synthesis solutions of NaBH₄ (0.6 mM) and AgNO₃ (0.2 mM) + TSC precursor solutions used for standard synthesis. The concentration of TSC is varied from 0.003 to 0.2 mM. Jetmixing runs at standard main line and jet-line flowrates of 48 mL h⁻¹ are performed for each TSC concentration. The Ag NP samples produced are analyzed by UV-vis 15 minutes after collection, as shown in Fig. S10.† For the Ag NP sample with 0.05 mM TSC, the FWHM calculated from the UV-vis spectrum comes out to be 58 nm, greater than the FWHM achieved for a comparable jet-mixing run without any salt addition (i.e., 52 nm). Similarly, for the Ag NP sample with 0.2 mM TSC, the FWHM calculated is 63 nm, significantly higher than that achieved for a standard jet-mixing synthesis without NaNO₃ (57 nm). This observation suggests the PSD is broadening.

This is also observed in Fig. S11† showing Ag NP solutions prepared at TSC concentrations of 0.01 mM, 0.05 mM and 0.2 mM. The gray color of the Ag NP solution synthesized using 0.01 mM TSC corroborates the aggregation of Ag and shows the presence of Ag in the form of bulk silver. The color of the solution blue-shifts from gray to yellow on increasing the TSC concentration. The blue-shift demonstrates the presence of smaller particles as the TSC concentration is increased.

While these results indicate that pre-synthetic addition of NaNO₃ to the Ag NP precursor solutions promotes ag-

glomeration of the synthesized Ag NPs, it is possible that addition of the salt before synthesis can alter the kinetics of the reduction of AgNO₃. Specifically, an increase in the NO₃ and Na ions in solution may affect the rate of conversion of Ag⁺ to Ag⁰, because of the common ion effect. To account for this, the standard jet-mixing synthesis at 0.2 mM TSC is repeated, but with 32 mM NaNO3 added postsynthesis to the Ag NP solution. The resultant mixture is analyzed by UV-vis and TEM. The UV-vis spectrum of the Ag NP sample before and after addition of 32 mM NaNO3 is shown in Fig. S12.† It is noticed that the spectrum broadens after addition of the salt, and the wavelength of maximum absorbance red-shifts, indicating formation of larger particles. Further, the absorbance of the UV-vis spectrum drops after salt addition, suggesting that the Ag NPs decrease in number, indicating increased aggregation. This observation is corroborated by the TEM image of the sample in Fig. S13† that shows the presence of large aggregates. To further validate our conclusion, these experiments were repeated for a higher concentration (64 mM) of NaNO3. The results for these have also been shown in Fig. S12 and S13† and confirm the previous results for 32 mM NaNO3. These experiments demonstrate that an increase in the ion concentration of the Ag NP solution caused by the addition of excess TSC could indeed increase the sample polydispersity. Hence, limiting the TSC concentration used in synthesis is not only beneficial in reducing the cost of synthesis, but also producing NPs with a more monodisperse PSD.

3.5. Stability of Ag NPs synthesized by batch and jet-mixing at optimum TSC concentration

An important consideration for the synthesis of Ag NPs is stability. While it is desirable to reduce the amount of capping agent used, the resultant nanoparticles should also be stable in solution. To analyze nanoparticle stability, the batch and jet-mixing solutions synthesized with 0.05 mM TSC at otherwise standard conditions are monitored over a long-term period. Each solution is divided into two separate samples post-synthesis to check similarity in growth profiles between identical samples. Further, two separate syntheses for batch and jet-mixing each are also performed for reproducibility. Equal volumes of each sample are stored in the refrigerator at 4 °C to prevent TSC degradation. The samples are evenly covered with aluminum foil to keep out external light. The FWHM of the samples is monitored via UV-vis at fixed intervals, starting from 15 minutes up to 1 month after synthesis. The FWHMs obtained for both batch and jet-mixing samples at each time of analysis are plotted in Fig. 9. Values for FWHM for batch and jet-mixingsynthesized samples have been listed in Tables S8 and S9,† respectively. While the FWHM for both batch and jet-mixing increase with time, the batch synthesized sample starts out with a broad FWHM as compared to the jet-mixing synthesized sample and remains so throughout the period of monitoring. The FWHM of the jet-mixing-synthesized sample,

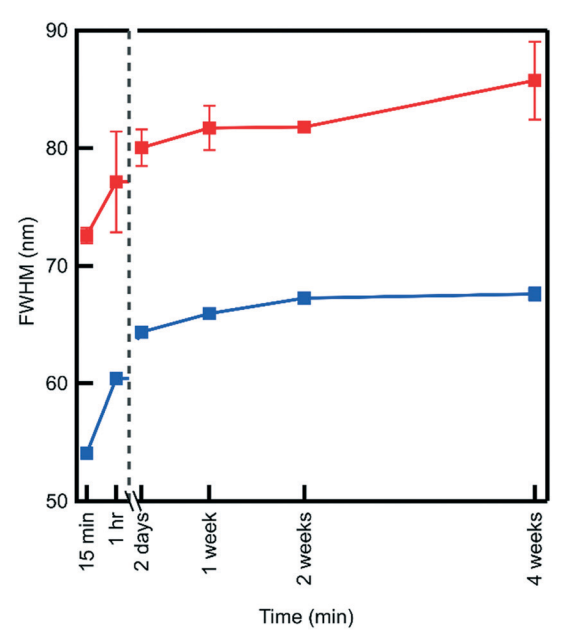


Fig. 9 FWHM obtained via UV-Vis for standard Ag NP batch (red) and jet-mixing (blue) synthesis with 0.05 mM TSC, plotted against different times of analysis post-synthesis from 15 minutes to 1 month. Other synthesis conditions are as follows: $Q_r = Q_j = 48 \text{ mL h}^{-1}$ for jet-mixing; $[NaBH_4] = 0.6 \text{ mM}, [AgNO_3] = 0.2 \text{ mM} \text{ for both syntheses}.$

after 1 month, is 18 nm smaller than the batch-synthesized sample. These results suggest that jet-mixing-synthesized samples at 0.05 mM TSC tend to remain monodisperse even on long storage.

4. Summary

A jet-mixing reactor is used to synthesize Ag NPs that are monodisperse (5 \pm 2 nm) with a narrow SPR peak. It is viable to produce Ag NP in large quantities by increasing reactor run-time, because of the consistent product quality produced and reproducible synthesis, as indicated by UV-vis. On varying the concentration of capping agent TSC in the jet-mixing synthesis, it is found that there is an optimum concentration of TSC (0.05 mM). At this optimum concentration, a monodisperse PSD is observed as suggested by a minimum SPR FWHM and corroborated using TEM images. This concentration of capping agent is lower by a factor of four than other reports while maintaining high quality particles. This optimum concentration provides balanced stabilization necessary to prevent agglomeration while maintaining a low solution ion concentration. It is shown that concentration higher than optimum results in destabilization of the solution by an increase in the ion concentration, causing Ag NP aggregation. External addition of NaNO₃ to the product solution also produces the same effect, confirming the hypothesis. With the lower concentration of capping agent of 0.05 mM, the nanoparticles produced using the jet-mixing reactor retain a narrower FWHM than the nanoparticles produced in the batch process. Overall, the jet-mixing reactor provides an efficient way to produce monodisperse particles in a continuous manner.

Notation

- Solution flowrate in the main line
- The solution flowrate in the jet line
- [A] Molar concentration of species A in solution

Conflicts of interest

There are no conflicts to declare.

Acknowledgements

The authors would like to acknowledge funding from the National Science Foundation (CBET 1653587) and The Ohio State University Institute of Materials Research (EMR-G00018 and IMR-FG0211). Images presented in this report were generated using the instruments and services at the Campus Microscopy and Imaging Facility, The Ohio State University. This facility is supported in part by grant P30 CA016058, National Cancer Institute, Bethesda, MD. The authors would also like to acknowledge Mariah Whitaker, Abhilasha Dehankar, and Kilho Lee for useful discussions.

References

- 1 X. Wu, P. L. Redmond, H. Liu, Y. Chen, M. Steigerwald and L. Brus, J. Am. Chem. Soc., 2008, 130, 9500-9506.
- 2 R. L. Hartman, J. P. McMullen and K. F. Jensen, Angew. Chem., Int. Ed., 2011, 50, 7502-7519.
- 3 N. T. K. Thanh, N. Maclean and S. Mahiddine, Chem. Rev., 2014, 114, 7610-7630.
- 4 R. Bakhtiar, J. Chem. Educ., 2013, 90, 203-209.
- 5 C. A. Dos Santos, M. M. Seckler, A. P. Ingle, I. Gupta, S. Galdiero, M. Galdiero, A. Gade and M. Rai, J. Pharm. Sci., 2014, 103, 1931-1944.
- 6 N. L. Pacioni, C. D. Borsarelli, V. Rey and A. V. Veglia, Silver Nanoparticle Applications, 2015.
- Denkova, Optical characterization of plasmonic nanostructures: near-field imaging of the magnetic field of light, 2014, vol. 3168.
- 8 E. Petryayeva and U. J. Krull, Anal. Chim. Acta, 2011, 706, 8-24.
- 9 B. Calderon-Jimenez, G. F. Sarmanho, K. E. Murphy, A. R. Montoro and J. R. Vega-Baudrit, J. Res. Natl. Inst. Stand. Technol., 2017, 122, 1-10.
- 10 S. Agnihotri, S. Mukherji and S. Mukherji, RSC Adv., 2014, 4, 3974-3983.
- 11 M. S. Saleh, C. Hu and R. Panat, Sci. Adv., 2017, 3, e1601986.
- 12 L. M. Molina, S. Lee, K. Sell, G. Barcaro, A. Fortunelli, B. Lee, S. Seifert, R. E. Winans, J. W. Elam, M. J. Pellin, I. Barke, V. Von Oeynhausen, Y. Lei, R. J. Meyer, J. A. Alonso, A. Fraile, A. Kleibert, S. Giorgio, C. R. Henry, K. Meiwesbroer and S. Vajda, Catal. Today, 2011, 160, 116-130.

- 13 C. Petit, P. Lixon and M. P. Pileni, J. Phys. Chem., 1993, 97, 12974–12983.
- 14 B. Ajitha, Y. A. Kumar Reddy, P. S. Reddy, H.-J. Jeon and C. W. Ahn, *RSC Adv.*, 2016, 6, 36171–36179.
- 15 H. Fathi, J. P. Kelly, V. R. Vasquez and O. A. Graeve, *Langmuir*, 2012, 28, 9267–9274.
- 16 D. Singha, N. Barman and K. Sahu, J. Colloid Interface Sci., 2014, 413, 37–42.
- 17 J. D. Martin, L. Telgmann and C. D. Metcalfe, *Bull. Environ. Contam. Toxicol.*, 2017, **98**, 589–594.
- 18 R. A. French, A. R. Jacobson, B. Kim, S. L. Isley and R. L. E. E. Penn, *Environ. Sci. Technol.*, 2009, 43, 1354–1359.
- 19 A. Henglein and M. Giersig, J. Phys. Chem. B, 1999, 103, 9533–9539.
- 20 R. Southey, The Story of the Three Bears, Longman, Rees, etc., 1837.
- 21 S. Silvestrini, T. Carofiglio and M. Maggini, Chem. Commun., 2013, 49, 84–86.
- 22 Z. Niu and Y. Li, Chem. Mater., 2014, 26, 72-83.
- 23 M. Carboni, L. Capretto, D. Carugo, E. Stulz and X. Zhang, J. Mater. Chem. C, 2013, 1, 7540.
- 24 X. Dong, X. Ji, H. Wu, L. Zhao, J. Li and W. Yang, J. Phys. Chem. C, 2009, 113, 6573–6576.
- 25 J. Liu, P. Raveendran, Z. Shervani, Y. Ikushima and Y. Hakuta, *Chem. Eur. J.*, 2005, 11, 1854–1860.
- 26 A. Taleb, C. Petit and M. P. Pileni, Chem. Mater., 1997, 9, 950–959.
- 27 C. Petit, P. Lixon and M. P. Pileni, *J. Phys. Chem.*, 1993, 97, 12974–12983.
- 28 X. Z. Lin, A. D. Terepka and H. Yang, Nano Lett., 2004, 4, 2227–2232.
- 29 D. Paramelle, A. Sadovoy, S. Gorelik, P. Free, J. Hobley and D. G. Fernig, *Analyst*, 2014, 139, 4855.
- 30 T. C. Prathna, N. Chandrasekaran, A. M. Raichur and A. Mukherjee, *Colloids Surf.*, *B*, 2011, 82, 152–159.
- 31 B. Pietrobon and V. Kitaev, *Chem. Mater.*, 2008, **20**, 5186–5190.
- 32 S. T. He, Y. L. Liu and H. Maeda, *J. Nanopart. Res.*, 2008, **10**, 209–215.
- 33 S. Iravani, H. Korbekandi, S. V. Mirmohammadi and B. Zolfaghari, *Results Pharma Sci.*, 2014, 9, 385–406.
- 34 K. Sen Chou, Y. C. Chang and L. H. Chiu, *Ind. Eng. Chem. Res.*, 2012, 51, 4905–4910.
- 35 W. Zhang, X. Qiao, Q. Chen, Y. Cai and H. Chen, *Appl. Surf. Sci.*, 2012, 258, 5909–5913.
- 36 M. Wuithschick, B. Paul, R. Bienert, A. Sarfraz, U. Vainio, M. Sztucki, R. Kraehnert, P. Strasser, K. Rademann, F. Emmerling and J. Polte, *Chem. Mater.*, 2013, 25, 4679–4689.
- 37 L. Xu, J. Peng, M. Yan, D. Zhang and A. Q. Shen, *Chem. Eng. Process.*, 2016, 102, 186–193.
- 38 J. Polte, X. Tuaev, M. Wuithschick, A. Fischer, A. F. Thuenemann, K. Rademann, R. Kraehnert and F. Emmerling, ACS Nano, 2012, 6, 5791–5802.
- 39 S. Mülhopt, S. Diabaté, M. Dilger, C. Adelhelm, C. Anderlohr, T. Bergfeldt, J. Gómez de la Torre, Y. Jiang, E.

- Valsami-Jones, D. Langevin, I. Lynch, E. Mahon, I. Nelissen, J. Piella, V. Puntes, S. Ray, R. Schneider, T. Wilkins, C. Weiss and H.-R. Paur, *Nanomaterials*, 2018, 8, 311.
- 40 L. Mockus, J. J. Peterson, J. M. Lainez and G. V. Reklaitis, Org. Process Res. Dev., 2015, 19, 908–914.
- 41 B. K. Johnson and R. K. Prud'homme, AIChE J., 2003, 49, 2264–2282.
- 42 M. M. Alvarez, J. M. Zalc, T. Shinbrot, P. E. Arratia and F. J. Muzzio, AIChE J., 2002, 48, 2135–2148.
- 43 B. K. Johnson and R. K. Prud'homme, *Aust. J. Chem.*, 2003, 1021–1024.
- 44 R. L. Hartman and K. F. Jensen, Lab Chip, 2009, 9, 2495.
- 45 S. Marre and K. F. Jensen, *Chem. Soc. Rev.*, 2010, 39, 1183–1202.
- 46 J. M. Ottino, Phys. Fluids, 2010, 22, 1-12.
- 47 X. Z. Lin, X. Teng and H. Yang, *Langmuir*, 2003, **19**, 10081–10085.
- 48 R. Baber, L. Mazzei, T. K. Thanh and A. Gavriilidis, RSC Adv., 2015, 5, 95585–95591.
- 49 R. Baber, L. Mazzei, N. T. K. Thanh and A. Gavriilidis, *Nanoscale*, 2017, 14149–14161.
- 50 D. V. R. Kumar, M. Kasture, A. A. Prabhune, C. V. Ramana, B. L. V. Prasad and A. A. Kulkarni, *Green Chem.*, 2010, 12, 609
- 51 K. S. Iyer, C. L. Raston and M. Saunders, *Lab Chip*, 2007, 7, 1800.
- 52 H. Mehenni, L. Sinatra, R. Mahfouz, K. Katsiev and O. M. Bakr, *RSC Adv.*, 2013, 3, 22397.
- 53 J. Boleininger, A. Kurz, V. Reuss and C. So, *Phys. Chem. Chem. Phys.*, 2006, 8, 3824–3827.
- 54 K. J. Hartlieb, M. Saunders, R. J. J. Jachuck and C. L. Raston, *Green Chem.*, 2010, 12, 1012.
- 55 D. Mitrakos, J. Jokiniemi, U. Backman and C. Housiadas, J. Nanopart. Res., 2008, 10, 153–161.
- 56 A. Günther, S. A. Khan, M. Thalmann, F. Trachsel and K. F. Jensen, *Lab Chip*, 2004, 4, 278–286.
- 57 A. Parulkar and N. A. Brunelli, *Ind. Eng. Chem. Res.*, 2017, 56, 10384–10392.
- 58 D. M. Holunga, R. C. Flagan and H. A. Atwater, *Ind. Eng. Chem. Res.*, 2005, 44, 6332–6341.
- 59 G. N. Glavee, K. J. Klabunde, C. M. Sorensen and G. C. Hadjapanayis, *Langmuir*, 1992, 8, 771–773.
- 60 K.-J. Wu, G. M. De Varine Bohan and L. Torrente-Murciano, *React. Chem. Eng.*, 2017, 2, 116–128.
- 61 C. A. Schneider, W. S. Rasband and K. W. Eliceiri, *Nat. Methods*, 2012, 9, 671–675.
- 62 G. A. Patil, M. L. Bari, B. A. Bhanvase, V. Ganvir, S. Mishra and S. H. Sonawane, *Chem. Eng. Process.*, 2012, 62, 69–77.
- 63 S. D. Solomon, M. Bahadory, A. V. Jeyarajasingam, S. A. Rutkowsky, C. Boritz and L. Mulfinger, *J. Chem. Educ.*, 2007, 84, 322–325.
- 64 R. Baber, L. Mazzei, N. T. K. Thanh and A. Gavriilidis, *J. Flow Chem.*, 2016, 6, 268–278.
- 65 J. F. A. de Oliveira and M. B. Cardoso, *Langmuir*, 2014, 30, 4879–4886.